additional *COR* genes in freezing tolerance. Whether CRT/DRE-containing *COR* genes are involved in bringing about the full array of biochemical and physiological changes that occur with cold acclimation (*1*, *2*) remains to be determined.

Freezing temperatures greatly limit the geographical distribution of native and cultivated plants and often cause severe losses in agricultural productivity (*16*). Traditional plant breeding approaches have met with limited success in improving the freezing tolerance of agronomic plants (*6*). The freezing tolerance of the best wheat varieties today is essentially the same as the most freezing-tolerant varieties developed in the early part of this century. Biotechnology, however, may offer new strategies. Here we show that the freezing tolerance of nonacclimated *Arabidopsis* plants is enhanced by increasing the expression of the *Arabidopsis* regulatory gene *CBF1*. The CRT/DRE DNA regulatory element we have targeted here is not limited to *Arabidopsis* (*17*) and thus may provide a way to improve the freezing tolerance of crop plants.

REFERENCES AND NOTES

1. C. L. Guy, *Annu. Rev. Plant Physiol. Plant Mol. Biol.* **41**, 187 (1990); M. A. Hughes and M. A. Dunn, *J. Exp. Bot.* **47**, 291 (1996).
2. M. F. Thomashow, in *Arabidopsis*, E. Meyerowitz and C. Somerville, Eds. (Cold Spring Harbor Laboratory Press, Plainview, NY, 1994), pp. 807–834.
3. S. S. Mohapatra, L. Wolfraim, R. J. Poole, R. S. Dhindsa, *Plant Physiol*. **89**, 375 (1989); M. Houde, R. S. Dhindsa, F. Sarhan, *Mol. Gen. Genet.* **234**, 43 (1992); C. Crosatti, E. Nevo, A. M. Stanca, L. Cattivelli, *Theor. Appl. Genet.* **93**, 975 (1996).
4. N. N. Artus *et al.*, *Proc. Natl. Acad. Sci. U.S.A.* **93**, 13404 (1996).
5. S. J. Gilmour and K. R. Jaglo-Ottosen, unpublished results.
6. M. F. Thomashow, *Adv. Genet.* **28**, 99 (1990).
7. R. K. Hajela, D. P. Horvath, S. J. Gilmour, M. F. Thomashow, *Plant Physiol.* **93**, 1246 (1990).
8. E. J. Stockinger, S. J. Gilmour, M. F Thomashow, *Proc. Natl. Acad. Sci. U.S.A.* **94**, 1035 (1997).
9. K. Yamaguchi-Shinozaki and K. Shinozaki, *Plant Cell* **6**, 251 (1994).
10. S. S. Baker, K. S. Wilhelm, M. F. Thomashow, *Plant Mol. Biol.* **24**, 701 (1994).
11. K. Nordin, T. Vahala, E. T. Palva, *ibid*. **21**, 641 (1993).
12. H. W. Wang, R. Datla, F. Georges, M. Loewen, A. Cutler, *ibid.* **28**, 605 (1995).
13. Standard procedures were used for plasmid manipulations (*18*). The CBF1-containing Ase I–Bgl II fragment from pACT-Bgl+ (*8*) was gel purified, Bam HI linkers were ligated to both ends, and the fragment was inserted into the Bam HI site in pCIB710 [S. Rothstein *et al.*, *Gene* **53**, 153 (1987)], which contains the CaMV 35*S* RNA promoter and terminator. The chimeric plasmid was linearized at the Kpn I site and inserted into the Kpn I site of the binary vector pCIB10g (Ciba-Geigy, Research Triangle Park, NC). The plasmid was transformed into *Agrobacterium tumefaciens* strain C58C1(pMP90) by electroporation. *Arabidopsis* plants were transformed by the vacuum infiltration procedure [N. Bechtold, J. Ellis, G. Pelletier, *C. R. Acad. Sci. Ser. III Life Sci.* **316**, 1194 (1993)] as modified [A. van Hoof and P. J. Green, *Plant J.* **10**, 415 (1996)].
14. A. M. Metz, R. T. Timmer, K. S. Browning, *Gene* **120**, 313 (1992).
15. N. P. Sukumaran and C. J. Weiser, *HortScience* **7**, 467 (1972).
16. W. Larcher, in *Physiological Processes Limiting Plant Productivity*, C. D. Johnson, Ed. (Butterworths, London, 1981), pp. 253–269; W. Larcher and H. Bauer, in *Physiological Plant Ecology I. Encyclopedia of Plant Physiology*, O. L. Lang, P. S. Nobel, C. B. Osmond, H. Ziegler, Eds. (Springer, Berlin, 1981), vol. 12, pp. 403–437.
17. C. Jiang, B. Iu, J. Singh, *Plant Mol. Biol.* **30**, 679 (1996).
18. J. Sambrook, E. F. Fritsch, T. Maniatis, *Molecular Cloning: A Laboratory Manual* (Cold Spring Harbor Laboratory Press, Cold Spring Harbor, NY, ed. 2, 1989).
19. S. J. Gilmour, R. K. Hajela, M. F. Thomashow, *Plant Physiol.* **87**, 735 (1988).
20. *Arabidopsis thaliana* ecotype RLD plants were grown in pots under continuous light (~100 μE m^{-2} s^{-1}) at 22°C for 18 to 25 days as described (*19*). In some cases, plants were then cold acclimated at 2.5°C under continuous light (~50 μE m^{-2} s^{-1}) for various amounts of time.
21. Total RNA was isolated from plant leaves and subjected to RNA blot analysis by high-stringency hybridization and wash conditions as described (*8, 19*). DNA probes were gel purified and radiolabeled with ^{32}P by random priming according to standard procedures (*18*).
22. Total soluble protein was isolated from plant leaves, fractionated by tricine SDS–polyacrylamide gel electrophoresis, and transferred to 0.2-μm nitrocellulose as described (*4*). COR15am protein was detected with antiserum raised to purified COR15am and protein A–conjugated alkaline phosphatase (Sigma) (*4*).
23. Electrolyte leakage tests were conducted as described (*15, 19*) with the following modifications. Two to four detached leaves from nonacclimated or cold-acclimated plants were placed in a test tube and submerged for 1 hour in a −2°C bath containing water and ethylene glycol in a completely randomized design, after which ice crystals were added to nucleate freezing. After an additional hour of incubation at −2°C, the samples were cooled in decrements of 1°C each hour. Samples (five replicates for each data point) were thawed overnight on ice and incubated in 3 ml of distilled water with shaking at room temperature for 3 hours. Electrolyte leakage from leaves was measured with a conductivity meter. The solution was then removed, the leaves were frozen at −80°C (for at least 1 hour), and the solution was returned to each tube and incubated for 3 hours to obtain a value for 100% electrolyte leakage.
24. Pots (9 cm) containing about 40 nonacclimated *Arabidopsis* plants (20 days old) and 4-day cold-acclimated plants (25 days old) (*20*) were placed in a completely randomized design in a −5°C cold chamber in the dark. After 1 hour, ice chips were added to each pot to nucleate freezing. Plants were removed after 2 days and returned to a growth chamber at 22°C.
25. Model curves fitting up to third-order linear polynomial trends were determined for each electrolyte leakage experiment. To ensure unbiased predictions of electrolyte leakage, trends significantly improving the model fit at the 0.2 probability level were retained. EL$_{50}$ values were calculated from the fitted models. An unbalanced one-way analysis of variance, adjusted for the different number of EL$_{50}$ values for each plant type, was determined by using SAS PROC GLM [SAS Institute, *SAS/STAT User's Guide, Version 6* (SAS Institute, Cary, NC, 1989)].
26. We wish to thank J. Dodgson, B. Sears, T. Deits, and E. Stockinger for critical reading of the manuscript. This research was supported in part by grants to M.F.T. from the National Science Foundation (IBN 9307348), the U.S. Department of Agriculture/National Research Initiative Competitive Grants Program (96-35100–3231), and the Michigan Agricultural Experiment Station.

14 October 1997; accepted 10 February 1998

Structural Conservation in Prokaryotic and Eukaryotic Potassium Channels

Roderick MacKinnon,* Steven L. Cohen, Anling Kuo, Alice Lee, Brian T. Chait

Toxins from scorpion venom interact with potassium channels. Resin-attached, mutant K$^+$ channels from *Streptomyces lividans* were used to screen venom from *Leiurus quinquestriatus hebraeus*, and the toxins that interacted with the channel were rapidly identified by mass spectrometry. One of the toxins, agitoxin2, was further studied by mutagenesis and radioligand binding. The results show that a prokaryotic K$^+$ channel has the same pore structure as eukaryotic K$^+$ channels. This structural conservation, through application of techniques presented here, offers a new approach for K$^+$ channel pharmacology.

Scorpion toxins inhibit ion conduction through potassium channels by occluding the pore at the extracellular opening. A single toxin protein binds very specifically to a single K$^+$ channel to cause inhibition. The toxins are 35 to 40 amino acids in length and have a characteristic fold that is held rigidly by three disulfide bridges (*1*). They are active site inhibitors, because when they bind to the channel they interact energetically with K$^+$ ions in the pore (*2–4*). The interaction between these inhibitors and the pore of K$^+$ channels has been exploited to gain insights into the structure and function of K$^+$ channels.

Studies employing site-directed mutagenesis of the Shaker K$^+$ channel have mapped the scorpion toxin binding site to regions corresponding to the extracellular entryway of the K$^+$ channel from *Streptomyces lividans* (the KcsA channel) (*4–9*). Although the amino acids of the K$^+$ channel selectivity filter are highly conserved, the residues lining the entryway are quite variable. As if to mirror the amino acid variation at the binding site, the toxins are also highly variable in

their amino acid composition. A given scorpion venom is a veritable library of toxins, apparently ensuring that a scorpion will inhibit a large fraction of K$^+$ channel types in its victim. Studies on the specificity of toxin-channel interactions have led to the following understanding: The extracellular entryway to the K$^+$ channel is relatively conserved in its three-dimensional structure but the precise amino acid composition is not conserved. The scorpion toxins have a shape, dictated by their conserved fold, that enables them to fit snugly into the entryway, but the affinity of a given toxin-channel pair depends on the residue match (or mismatch) on both interaction surfaces.

We have studied the interaction between the KcsA K$^+$ channel (5) and the scorpion toxin agitoxin2 (10). By producing, through mutagenesis, a competent toxin binding site, we show that the KcsA K$^+$ channel pore structure and extracellular entryway are very similar to that of eukaryotic voltage-gated K$^+$ channels such as the *Shaker* K$^+$ channel from *Drosophila* and the vertebrate voltage-gated K$^+$ channels. By combining our extensive functional data on the toxin-channel interaction with the structures of both proteins we propose a highly-restrained model of the complex structure.

Guided by knowledge of the toxin receptor on the *Shaker* K$^+$ channel, we introduced three point mutations into the KcsA K$^+$ channel that should render it sensitive to scorpion toxins (Fig. 1). Amino acids 61 and 64 were changed to their *Shaker* K$^+$ channel counterpart and 58 was changed to Ala since a small side chain at this latter position favors binding (4, 7). The mutant KcsA K$^+$ channel was expressed in *Escherichia coli*, extracted from the membrane with the detergent decylmaltoside, and bound to cobalt resin through a carboxyl terminal hexahistidine tag (11). A 1-ml column, prepared with the K$^+$ channel–containing resin, was used to screen the venom of the scorpion *Leiurus quinquestriatus hebraeus*, the source of numerous well-characterized ion channel toxins. Forty milligrams of venom was added to the column and, after washing, the K$^+$ channel was eluted with an imidazole solution (12). The eluate was analyzed with MALDI-TOF mass spectrometry, focusing on the low mass range appropriate for scorpion toxins

(∼4000 daltons). Passage of the venom over the K$^+$ channel column resulted in a dramatic enhancement of specific peaks (Fig. 2, A through C). Three of these corresponded in mass to the known K$^+$ channel toxins agitoxin2, charybdotoxin, and Lq2 (Fig. 2, C and D). A fourth peak (Fig. 2C, asterisk) apparently represents a previously unknown toxin. The peak corresponding to chlorotoxin, a chloride channel inhibitor (13), did not bind to the column (Fig. 2, A and C).

Further quantitative analysis was carried out with agitoxin2. Radiolabeled agitoxin2 was prepared by producing the mutation D20C in the toxin (located far from its channel binding surface) and conjugating it with tritiated *N*-ethylmaleimide (14). A filter assay showed that labeled agitoxin2 binds to the mutant KcsA K$^+$ channel with an equilibrium dissociation constant (K_D) of about 0.6 μM (Fig. 3A). In contrast, no binding to the wild-type channel could be detected. The total capacity of resin saturated with mutant channel, based on the specific activity of radiolabeled toxin and the known 1:1 stoichiometry (one toxin per tetrameric channel), is nearly 50 pmol of

channel per microliter of resin. This value approximates the expected capacity of the resin and therefore implies that all of the channels in the preparation have a correct conformation.

Amino acids in a well-defined region of agitoxin2 form its functional interaction surface, as determined by the effects of alanine substitution on binding to the *Shaker* K$^+$ channel [Fig. 3C (4, 8)]. Mutation of Lys^{27} and Asn^{30} had the largest destabilizing effects. Lys^{27} is conserved in all members of this toxin family because its side chain apparently plugs the pore of K$^+$ channels (3). To confirm that agitoxin2 uses the same amino acids to interact with the mutant KcsA K$^+$ channel, we studied the effects of the K27A and N30A toxin mutations with a competition binding assay (Fig. 3B). These mutations decreased the affinity for the toxin significantly (130-fold and 45-fold, respectively), as anticipated from the *Shaker* K$^+$ channel studies. In contrast, the D20C mutation (predicted to be on the back side of the toxin), even with a bulky *N*-ethylmaleimide adduct, did not influence affinity (Fig. 3, A and B). These results show that agi-
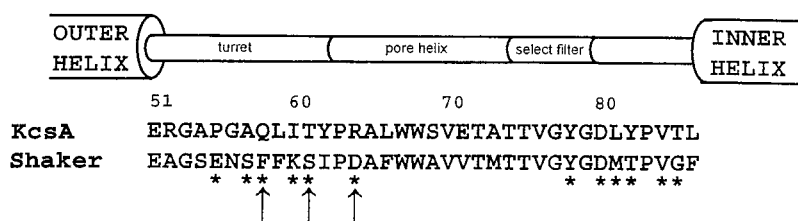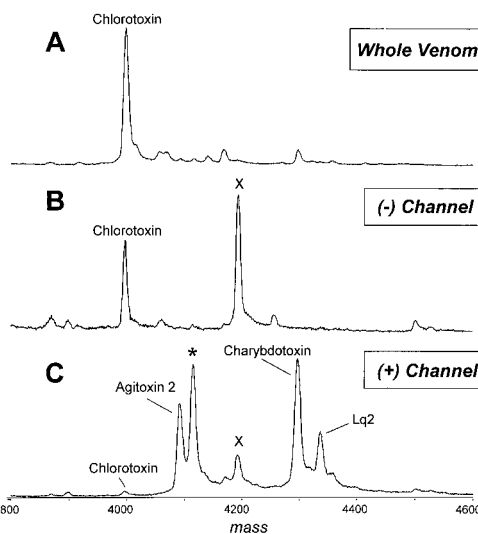

Fig. 1. Sequence alignment of the KcsA and *Shaker* K$^+$ channel pore regions. The numbering for KcsA is above the sequences. Structural elements are indicated (5). Asterisks, several *Shaker* K$^+$ channel amino acid locations where mutations influence agitoxin2 binding (4, 8, 9); arrows, the three KcsA K$^+$ channel amino acids mutated in this study. The sequences are KcsA, *S. lividans*, accession number (acc) PIR S60172; and *Shaker*, *Drosophila melanogaster*, acc PIR S00479.

R. MacKinnon and A. Kuo, Laboratory of Molecular Neurobiology and Biophysics and the Howard Hughes Medical Institute, Rockefeller University, 1230 York Avenue, New York, NY 10021, USA.
S. L. Cohen and B. T. Chait, Laboratory of Mass Spectrometry and Gaseous Ion Chemistry, Rockefeller University, 1230 York Avenue, New York, NY 10021, USA.
A. Lee, Laboratory of Molecular Neurobiology and Biophysics, Rockefeller University, 1230 York Avenue, New York, NY 10021, USA.

*To whom correspondence should be addressed. E-mail: mackinn@rockvax.rockefeller.edu

D

Toxin	Mass (Da)	
	Measured	Calculated
Chlorotoxin	3996.4	3996.7
Agitoxin 2	4090.8	4090.9
*	4113.5	––––––
Charybdotoxin	4295.9	4296.0
Lq2	4336.1	4336.0

Fig. 2. Mass spectra of scorpion toxins before and after purification on a K$^+$ channel column. MALDI-TOF mass spectra of venom before purification (**A**) and after elution from a cobalt column in the absence (**B**) and presence (**C**) of attached mutant KcsA K$^+$ channel. The accuracy of the mass measurements (±0.3 dalton) permitted identification of most of the major peaks in the mass spectra searched from databases of known toxins of the *L. quinquestriatus hebraeus* scorpion (**D**). The KcsA-binding component labeled with an asterisk could not be assigned to a known scorpion toxin. The component labeled X (4193.0 daltons) binds nonspecifically to the column and was not identified. MALDI-MS was performed with the MALDI matrix 4-hydroxy-α-cyano-cinnamic acid (16).

toxin2 binds in the same manner to both the mutant KcsA K+ channel and the *Shaker* K+ channel. The affinity for the *Shaker* K+ channel is considerably higher (K_D 1 nM), but we have only mutated three amino acids to mimic the site on the *Shaker* K+ channel (Fig. 1).

These results demonstrate that the overall structure of the agitoxin2 receptor site is very similar on both the KcsA and *Shaker* K+ channels. This conclusion justifies the use of energetic data borrowed from *Shaker* K+ channel studies to assist in the docking of agitoxin2 onto the KcsA K+ channel structure. Thermodynamic mutant cycle analysis has allowed the identification of numerous energetically coupled residue pairs on the interface [pairs of residues that are related by the fact that mutating one influences the effect (on equilibrium binding) of mutating the other (8)]. The four best defined of these residue pairs are displayed in matched colors on the KcsA K+ channel and agitoxin2 surfaces (Fig. 4A). The three off-center residue

pairs (blue, green, yellow) have the strongest mutant cycle coupling energies [>3 kT (4, 8)]. The central residue pair (red) is coupled by 1.7 kT and independent information places Lys^{27} (red residue on agitoxin2, Fig. 3A) over the pore (3, 4). Mere visual inspection suggests a unique orientation for the toxin on the channel (Fig. 4B). If the toxin is placed with its functionally defined interaction surface face-down in the groove formed by the turrets (5), with Lys^{27} at the center, the colors match well in three dimensions. The toxin seems to fit perfectly into the vestibule of a K+ channel. The four-fold symmetry of the K+ channel provides four statistically distinguishable but energetically identical orientations available for a toxin to bind [(Fig. 4A) (15)].

In summary, through a combination of structural and functional data we present a view of a K+ channel in complex with a neurotoxin from scorpion venom. The KcsA K+ channel is structurally very similar to eukaryotic K+ channels. This struc-

tural conservation, through application of techniques developed here, can be exploited to advance our understanding of K+ channel pharmacology.

REFERENCES AND NOTES

1. M. L. Garcia *et al.*, *J. Bioenerg. Biomembr*. **23**, 615 (1991); C. Miller, *Neuron* **15**, 5 (1995).
2. R. MacKinnon and C. Miller, *J. Gen. Physiol*. **91**, 335 (1988); K.M. Giangiacomo, M. L. Garcia, O. B. McManus, *Biochemistry* **31**, 6719 (1992).
3. C. S. Park and C. Miller, *Neuron* **9**, 307 (1992).
4. R. Ranganathan, J. H. Lewis, R. MacKinnon, *ibid*. **16**, 131 (1996).
5. D. A. Doyle *et al.*, *Science* **280**, 69 (1998).
6. R. MacKinnon and C. Miller, *ibid*. **245**, 1382 (1989); R. MacKinnon, L. Heginbotham, T. Abramson, *Neuron* **5**, 767 (1990); M. Stocker and C. Miller, *Proc. Natl. Acad. Sci. U.S.A.* **91**, 9509 (1994); D. Naranjo and C. Miller, *Neuron* **16**, 123 (1996).
7. S. Goldstein, D. J. Pheasant, C. Miller, *Neuron* **12**, 1377 (1994).
8. P. Hidalgo and R. MacKinnon, *Science* **268**, 307 (1995).
9. A. Gross and R. MacKinnon, *Neuron* **16**, 399 (1996).
10. M. L. Garcia *et al.*, *Biochemistry* **33**, 6834 (1994).
11. Three mutations (Q58A, T61S, and R64D) were introduced into the KcsA K+ channel gene to modify its pore region sequence by PCR mutagenesis and confirmed by DNA sequencing. The gene also contained a mutation at the second residue (P2A) to introduce an Nco I restriction endonuclease site, and it was lacking the last two carboxyl-terminal residues. This gene was cloned into the pQE60 vector for expression with a carboxyl terminal thrombin and hexahistidine fusion. Channel protein was expressed in XL-1 Blue strain of *E. coli* (Stratagene) by induction with 1-β-D-thiogalactopyranoside at a concentration of 1.0 mM. Three hours after induction, bacteria were sonicated in 50 mM tris buffer (pH 7.5), 100 mM KCl, 10 mM Mg₂SO₄, 25 mg deoxyribonuclease 1, and 250 mM sucrose, plus pepstatin, leupeptin, and PMSF. The channel was extracted in the same solution containing 40 mM decylmaltoside (Anatrace) at room temperature. Following centrifugation the supernatant was bound to cobalt resin (Talon) at a protein to resin ratio that will saturate the resin. The resin was washed, and detergent concentration was lowered to 10.0 mM. One-milliliter columns were prepared. The control resin (no channel) was handled in the same manner. The resin preparation was the same for mass spectrometry and binding studies.
12. Forty milligrams of *L. quinquestriatus hebraeus* venom (Alomone Labs) was suspended in buffer identical to that of the channel (10.0 mM decylmaltoside) and applied to the column. After washing, channel was eluted with 1.0 M imidazole in the same buffer.
13. J. A. Debin, J. E. Maggio, G. R. Strichartz, *Am. J. Physiol. Soc.* **264**, C369 (1993); G. Lippens, J. Najib, S. J. Wodak, A. Tartar, *Biochemistry* **34**, 13 (1995).
14. S. K. Aggarwal and R. MacKinnon, *Neuron* **16**, 1169 (1996).
15. R. MacKinnon, *Nature* **350**, 232 (1991).
16. S. L. Cohen and B. T. Chait, *Anal. Chem.* **68**, 31 (1996).
17. Wild-type and mutant agitoxin2 were prepared (10). Tritiated *N*-ethylmaleimide (NEN Life Sciences) was conjugated to agitoxin2 D20C (14). Binding was performed in a 300-µl volume containing 50 mM tris, 100 mM KCl, 10 mM decylmaltoside, and 0.3 µl of cobalt resin saturated with the mutant KcsA K+ channel for 30 min at room temperature. After brief centrifugation, the supernatant was removed. Resin was applied to a filter and rinsed briefly with ice-cold buffer; radioactivity was then determined in a scintillation counter. All binding measurements were made with a paired control containing a saturating concentration (200 times K_D) of unlabeled wild-type agitoxin2 to determine nonspecific binding. The competition assay was carried out under the same conditions. Labeled agitoxin2 at 0.06 µM was always present and unlabeled toxin was added to compete with bound labeled toxin.
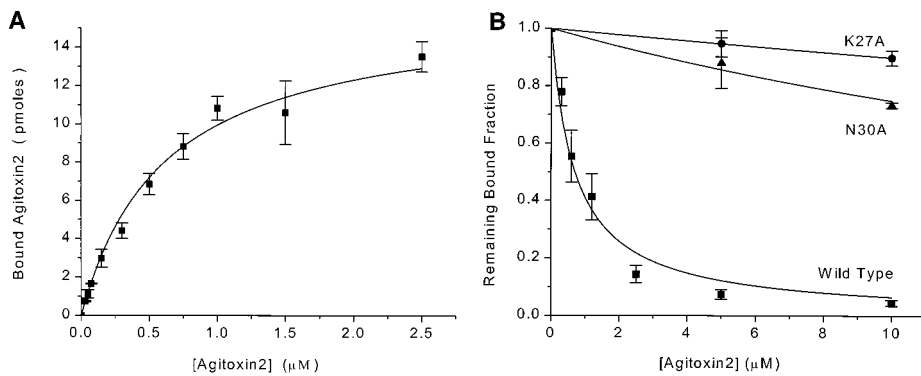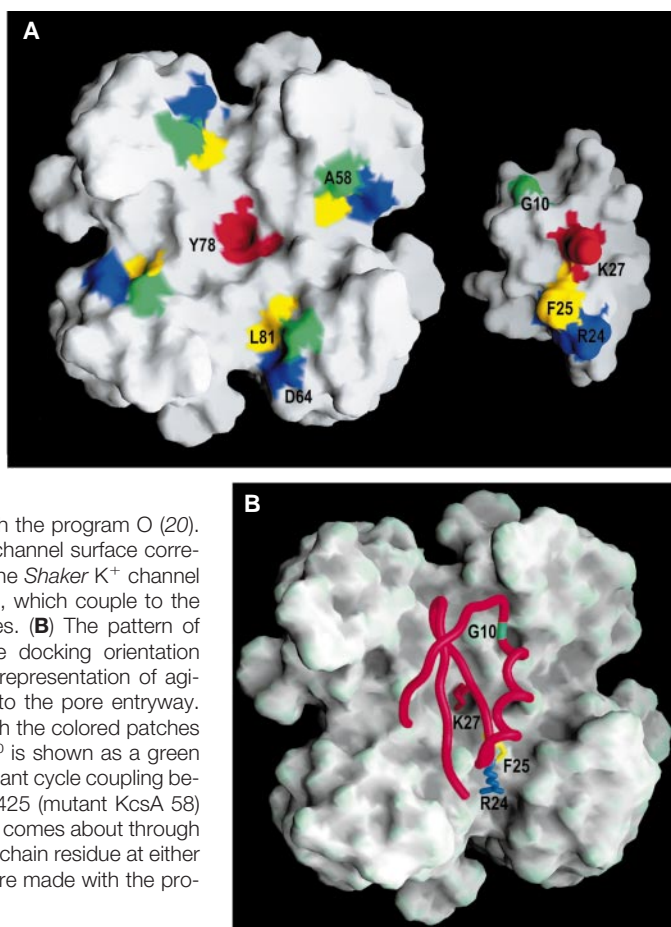
Fig. 3. Binding affinity of wild-type and mutant agitoxin2 to the mutant KcsA K+ channel. (**A**) Quantity of radiolabeled agitoxin2 bound to 0.3 µl of cobalt resin saturated with the mutant KcsA K+ channel as a function of the radiolabeled agitoxin2 concentration (17). Each point is the mean ±SEM of four measurements, except for the 0.03 µM and 1.5 µM concentrations, which are the mean ± range of mean of two measurements. The curve corresponds to equation: bound agitoxin2 = $A \times \{1 + K_D/[agitoxin2]\}^{-1}$, with equilibrium dissociation constant K_D = 0.62 µM and resin capacity A = 16 pmol. (**B**) Remaining bound fraction of radiolabeled wild-type toxin as a function of the concentration of unlabeled wild-type toxin or mutant toxins K27A or N30A (17). Each point is mean ± SEM of four measurements for wild-type agitoxin2 (squares) or mean ± range of mean of two measurements for K27A (circles) and N30A (triangles) agitoxin2 mutants. The curves correspond to equation: remaining bound fraction = $\{1 + K_{Dhot}/[agitoxin2_{hot}]\} \times \{1 + (K_{Dhot}/[agitoxin2_{hot}]) \times (1 + [agitoxin2_{cold}]/K_{Dcold})\}^{-1}$ with labeled toxin concentration $[agitoxin2_{hot}]$ = 0.06 µM, wild-type toxin K_{Dhot} = 0.62 µM, and competing toxin dissociation constant K_{Dcold} = 0.62 µM (wild type), 81 µM (K27A), and 27 µM (N30A). (**C**) CPK model of the interaction surface of agitoxin2 (18). Side chains of functionally important amino acids are in red (4). This figure was prepared with the program GRASP (19).

Fig. 4. Docking of agitoxin2 onto the KcsA K$^+$ channel. (**A**) Molecular surface of the pore entryway of the KcsA K$^+$ channel (left) and agitoxin2 (right). The colors indicate locations of interacting residues on the toxin and channel surfaces as determined by thermodynamic mutant cycle analysis of the *Shaker* K$^+$ channel-agitoxin2 interaction (*4*, *8*). The three pore mutations of the KcsA K$^+$ channel used in this study (Q58A, T61S, and R64D) were introduced into the channel model with the program O (*20*). Indicated residues on the channel surface correspond to the positions of the *Shaker* K$^+$ channel equivalent residues (Fig. 1), which couple to the indicated agitoxin2 residues. (**B**) The pattern of colors in (A) suggests the docking orientation shown by the main chain representation of agitoxin2 placed manually onto the pore entryway. The side chain colors match the colored patches in (A). The position of Gly^{10} is shown as a green band on agitoxin2. The mutant cycle coupling between residues at *Shaker* 425 (mutant KcsA 58) and residue 10 of agitoxin2 comes about through substitution of a bulky side chain residue at either position (*4*, *7*). Pictures were made with the program GRASP (*19*).

18. A. M. Krezel *et al.*, *Prot. Sci.* **4** 1478 (1995).
19. A. Nicholls, K. A. Sharp, B. Honig, *Proteins* **11**, 281 (1991).
20. T. A. Jones, J. Y. Zou, J. Y. Cowan, M. Kjeldgaard, *Acta Crystallogr.* **A47**, 110 (1991).
21. We thank J. Gulbis, J. P. Imredy, and D. A. Doyle for assistance in preparation of the figures and helpful discussions on the work. Supported by NIH GM43949. R.M. is an investigator in the Howard Hughes Medical Institute.

6 March 1998; accepted 13 March 1998

Requirement of Ras-GTP–Raf Complexes for Activation of Raf-1 by Protein Kinase C

Richard Marais, Yvonne Light, Clive Mason, Hugh Paterson, Michael F. Olson, Christopher J. Marshall*

Receptor tyrosine kinase–mediated activation of the Raf-1 protein kinase is coupled to the small guanosine triphosphate (GTP)–binding protein Ras. By contrast, protein kinase C (PKC)–mediated activation of Raf-1 is thought to be Ras independent. Nevertheless, stimulation of PKC in COS cells led to activation of Ras and formation of Ras–Raf-1 complexes containing active Raf-1. Raf-1 mutations that prevent its association with Ras blocked activation of Raf-1 by PKC. However, the activation of Raf-1 by PKC was not blocked by dominant negative Ras, indicating that PKC activates Ras by a mechanism distinct from that initiated by activation of receptor tyrosine kinases.

The PKC family of lipid-dependent Ser-Thr kinases has at least 11 members (*1*). The typical and atypical PKC isozymes are activated by diacylglycerol (DAG), which is produced by the metabolism of phosphatidyl inositols. In the case of 7-transmembrane (7-TM) receptors that are coupled to the heterotrimeric guanosine nucleotide–binding protein (G protein) Gαq, DAG is generated by the activation of

phospholipase C-β (PLC-β) (*2*). Both the typical and atypical PKCs are activated by phorbol esters. Activation of PKC leads to short-term responses such as altered metabolic activity and to long-term responses such as differentiation or effects on proliferation and apoptosis (*1*). The extracellular signal–regulated kinases (ERKs) are mitogen-activated protein kinases (MAPKs), which are activated by PKC (*3–7*) and appear to mediate the effects of PKC on differentiation, secretion, proliferation, and hypertrophy (*8*). Signaling from receptor tyrosine kinases to ERKs is dependent on Ras proteins and the protein kinase Raf-1 (*9*). However, the role of Ras in transducing signals from PKC to the ERKs is unclear, because expression of a dominant negative Ras in which amino acid 17 is changed to Asn (N17Ras) does not block ERK activation by PKC in a number of cell types (*4, 5*). This Ras mutant, which is thought to function by inhibiting guanine nucleotide exchange factors (*10*), blocks activation of ERKs in response to stimulation of receptor tyrosine kinases in many cell types (*4–6*).

To investigate whether PKC activates the ERK MAPK pathway by a mechanism independent of Ras, we used a monkey kidney cell line (COS cells), because in these cells, N17Ras does not block PKC-mediated ERK activation (*4*). We blocked Ras signaling by microinjection of the Ras-neutralizing monoclonal antibody Y13-259 (*11*). To detect ERK activation, we used an antibody that recognizes only the dually phosphorylated, active form of ERK. Activation of ERK in COS cells treated with 12-O-tetradecanoyl-phorbol-13-acetate (TPA) was completely blocked by microinjection of Y13-259 (Fig. 1). This demonstrates an essential role for Ras in activation of the ERK MAPK cascade by PKC. These data are consistent with studies on overexpression of Ras guanosine triphosphatase–activating protein (p120Ras-GAP), which blocks TPA-stimulated activation of ERKs, although it is unclear in those studies whether the p120Ras-GAP was acting on Ras or a related protein (*7*).

To further investigate whether Ras has a role in activation of Raf-1 by PKC, we used a mutant Raf-1 protein in which Arg^{89} is replaced with Leu (R89LRaf-1). This mutant does not bind the GTP-bound form of Ras (Ras-GTP) (*12*). Unlike transiently expressed wild-type Raf-1 (mRaf-1), R89LRaf-1 was not activated in cells treated with TPA (Fig. 2A). Exogenous mRaf-1 was activated with similar

CRC Centre for Cell and Molecular Biology, Institute of Cancer Research, 237 Fulham Road, London SW3 6JB, UK.

*To whom correspondence should be addressed. E-mail: chrism@icr.ac.uk